Lasers in Manufacturing Conference 2023

# Improving the absorption of copper for near-infrared laser beams to optimize laser spot welding quality of copper to aluminum

Mahdi Amne Elahi[a,*], Mohammadhossein Norouzian[a], Peter Plapper[a]

[a]*University of Luxembourg, 6, rue Coudenhove-Kalergi, Luxembourg L-1359, Luxembourg*

**Abstract**

Laser spot welding of copper-aluminum has gained significant attention thanks to the unique properties of these metals in addition to the capabilities of laser welding. Applying the laser on the aluminum side in an overlap configuration is well-studied in the literature however, directing the beam from the copper may bring some advantages to better control the final microstructure of the weld and minimize the formation of intermetallic compounds. The issue to be addressed is the considerable reflectivity of copper surfaces for well-established near-infrared laser sources. In this paper, the absorption of copper is improved by implementing laser-based surface structuring. The absorption of copper is tracked with online temperature measurement and offline microscopic observation. In addition, the shear load of welded copper-aluminum samples with different copper surface conditions and laser powers was considered to explain the absorption of the laser beam and optimize the microstructure of the weld zone regarding the formation of intermetallic compounds.

Keywords: laser welding of Cu-Al; laser beam absorption; intermetallic compounds; laser-based surface structuring

## 1. Introduction

Copper has recently emerged as a highly favored material in diverse industries. Scientific investigations represent a surge in copper use, alongside significant advancements in the parallel processing and producing techniques employed for this material. Due to copper's high inherent electrical conductivity, it plays a critical role in the automotive industry. Copper parts are essential electrical connecting elements inside the cell and

* Corresponding author. Tel.: +352-466644-5885.
*E-mail address:* mahdi.amneelahi@uni.lu.

peripheral electronics of the battery. Consequently, the high quality of the joining against thermal and mechanical stresses is essential. In addition, the rapid cycle time and the facilitation of extensive automation are crucial. Laser welding of dissimilar materials like copper and aluminum has been considered a promising technology for battery manufacturing (Brand et al., 2015). However, this procedure encounters several challenges related to copper's high reflectivity and low absorption characteristics in laser welding with a near-infrared wavelength. This simply leads to difficulty in keyhole formation (Hess et al., 2011). A lack of bonding with aluminum and an unstable weld may arise due to the high reflection of a laser beam with low energy input on the copper surface. (Dong and Xiao, 2009) concluded that consistent weld qualities could only be attained when the welding conditions exceeded a specific threshold of heat input. However, compensating for copper's reflectivity by increasing the energy coupling of the laser beam to change the solid/liquid phase can cause additional defects, such as melt ejections, intermetallic compounds (IMCs), voids, and cracks (Heider et al., 2015), (Norouzian et al., 2023). Moreover, laser welding materials with lower thickness increase the likelihood of encountering these defects. (Amne Elahi and Plapper 2019) studied the laser micro-welding of thin Nickel wire to CuSn6 bronze terminal for automotive application. A tight process window is defined based on optimum power and beam trajectory to avoid miscellaneous defects.

Several studies seek to overcome the copper reflectivity and increase the copper surface absorption rate. (Biro et al., 2002) investigated the utilization of oxygenated assist gases in the laser welding of copper. By introducing oxygen in the argon as the assist gas during laser welding, they observed the formation of an oxide layer on the surface of the copper sheet. This oxide layer increased the coupling effect between the laser beam and the copper surface, leading to a higher energy absorption rate. Consequently, the formation of keyholes was accelerated, and weld penetration increased. (Chen et al., 2015) implemented a copper-based nano-composite as an absorber material in laser welding processes. By applying it to pure copper specimens, they significantly reduced the reflectivity of the copper from an initial value of 88% to 15%. Furthermore, the authors observed that implementing the absorber material did not significantly change the weld's chemical composition or electrical conduction. Moreover, this approach enabled a wider and deeper weld zone, indicating favorable outcomes regarding weld quality. A study by (Steen and Mazumder, 2010) observed that applying a short wavelength laser beam in the laser welding of copper alloys leads to enhancing energy absorption and improving welding efficiency. They measured an increase in laser beam energy absorption, from approximately 3% to 40%, when the wavelength of the laser beam was shifted from 1000 nm to 500 nm. (Engler et al., 2011) compared the utilization of green and infrared laser radiation in the laser welding of copper. An examination of energy coupling and weld shape analysis showed that green radiation exhibited superior absorption properties in copper's liquid and solid states. Applying green radiation reduced the power threshold required for achieving deep welding.

Another method that allows using infrared laser radiation with almost 1000 nm wavelength is increasing the copper specimens' surface roughness to elevate the absorption. (Maina et al., 2018) created appropriate concave holes on the surface of copper. They concluded that the surface roughness with grooves around 30 µm leads to stabilized micro welding, deep penetration, and quality welding. (Kaierle et al., 2016) reported that enhancing the surface roughness of the copper specimens can reinforce the absorption of infrared laser radiation. Consequently, this treated copper surface can lead to the formation of a keyhole and promote deeper penetration during laser processing. (Helm et al., 2020) used a fiber laser with a 1070 nm wavelength for copper laser welding. However, to mitigate the reflectivity of this material, they considered a laser-structured surface before the welding. An 86% deduction of reflectance for a structured surface compared to as-received copper is reported. Their conclusions express that the surface structures generated before the

welding process can expedite the transition to a deep penetration laser welding process while increasing the energy input. (Lee and Ki, 2021) implemented femtosecond laser surface modification to alter the reflectance properties of copper surfaces, thereby welding procedure speeded up to 300%. This technique proved effective in mitigating the issue of heat loss during the copper welding process. By strategically laser texturing procedures at regular intervals along the welding direction, they successfully expanded the width of the weld zone. Importantly, this study confirms using infrared lasers for welding of modified surfaces, even for materials with exceptionally high reflectivity characteristics.

All these investigations have significantly contributed to comprehending copper's fundamental characteristics and the enhancements achieved in its absorption in laser welding. Nonetheless, further investigations are required to explore the significance of copper's surface structure, its consequential impact on the formation of metallurgical phases, and the mechanical strength of joints, specifically the joining of copper and aluminum (Cu-Al) with low thickness. Advancing our understanding in this area will provide valuable insights into optimizing the welding process and ensuring robust joints for Cu-Al welding. This article presents a laser-based structuring technique that aims to enhance Cu absorption properties for the industry economically. The study investigates surface roughness's impact on Cu absorption characteristics through experimental analysis. To gain comprehensive insights into the welding process, online temperature measurement is employed to analyze the temperature increment for varying surface roughness conditions. The ultimate objective is to establish a structured surface with enhanced absorption capabilities, ensuring to use of the minimum power during laser spot welding of low-thickness Cu-Al while providing a stable keyhole with the minimized formation of IMCs.

## 1. Experimental procedure

### *1.1. Laser-based surface structuring*

Surface structuring of the Cu samples is done with a pulse laser (TruMark 6030). The laser power was fixed at its maximum of 20 W; the focal position on the surface of the material; and the rest of the parameters concerning the surface structuring with the laser beam are shown in Table 1.

Table 1. Laser beam parameters concerning surface structuring of Cu.

| Sample code | Pulse Frequency (*kHz*) | Speed (*mm/s*) | Line spacing (*mm*) |
|---|---|---|---|
| **R1** | 100 | 350 | 0.05 |
| **R2** | 100 | 200 | 0.05 |
| **R3** | 100 | 170 | 0.05 |

### *1.2. Laser welding*

The present study used copper (oxide free, 99.95% pure) and aluminum (Al 1050) specimens. The dimensions of the samples and overlap welding configuration are presented in Fig. 1. Laser welding process is implemented with a fiber laser (TruFiber 400) equipped with a scanner head (Scanlab HS20 2D f-Θ scanner). The trajectory of the laser beam is a moving outward spiral shape with a diameter of 2 mm and the speed of 85 mm/s. The position of the tip of the thermocouple is fixed 1.5 mm below the center of the spiral for temperature measurements (see Fig. 1). The experiments were performed with different powers of 220, 228, and 240 watts which correspond to the power densities of $2.91 \times 10^7\ W/cm^2$, $3.02 \times 10^7\ W/cm^2$, and $3.18 \times 10^7\ W/cm^2$, respectively.

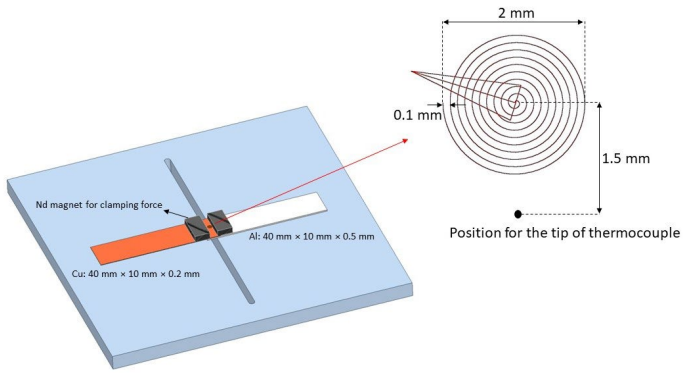


Fig. 1. Materials dimensions, welding configuration, and beam trajectory.

### *1.3. Temperature measurement, roughness measurement, microscopic evaluations, and mechanical testing*

To measure the temperature, a K-type thermocouple connected to Keithley DMM7510 digital multimeter recorded the temperature with a frequency of 230 Hz. The tip of the thermocouple is attached firmly to the surface of the specimen using Kapton tape.

The roughness values of the samples are measured with a surface roughness tester (TESA-rugosurf 10-G) in accordance with ISO 4287/JIS B0601, and the presented values are Ra (average surface roughness), Rp (maximum profile peak height), and Rv (maximum profile valley depth). It is worth mentioning that the roughness tests are done orthogonally to the direction of the laser-engraved lines, and the reported values are the average of at least five independent measurements.

Welded samples were cut accurately for metallographic sample preparation, followed by mounting in a thermoset resin and consecutive grinding and polishing steps. Several optical microscopic images were taken before and after etching with the solution, as described in Table 2.

Table 2. The etchant solution for the Al-Cu welded samples.

| Name | Chemical composition | Etching time |
|---|---|---|
| **ANPE 80/5/5/10** | $H_3PO_4$ (73%), $HNO_3$ (3.1%)<br>$CH_3COOH$ (3.3%), $H_2O$ (20.6%) | 30 s – 2 min |

The mechanical tests are done in the single-lap shear configuration using a Zwick/Roell tensile test machine with a maximum force of 5 kN. The reported values are the average of at least three independent measurements.

## 2. Results and Discussions

### *2.1. Surface structuring*

Fig. 2 illustrates the top and cross-sectional view of the as-received and laser-structured Cu surfaces across various samples. These samples can be assessed with the roughness analysis in Fig. 3. The surface roughness analysis presents the Rv, Rp, and Ra values for four classes. The graph includes error bars representing the standard deviation. Among them, the R3 class exhibited the most significant fluctuation. The average surface

deviation for this category was approximately 1.4 µm, with a maximum peak value of 3.9 µm and a maximum profile valley of 4.7 µm.

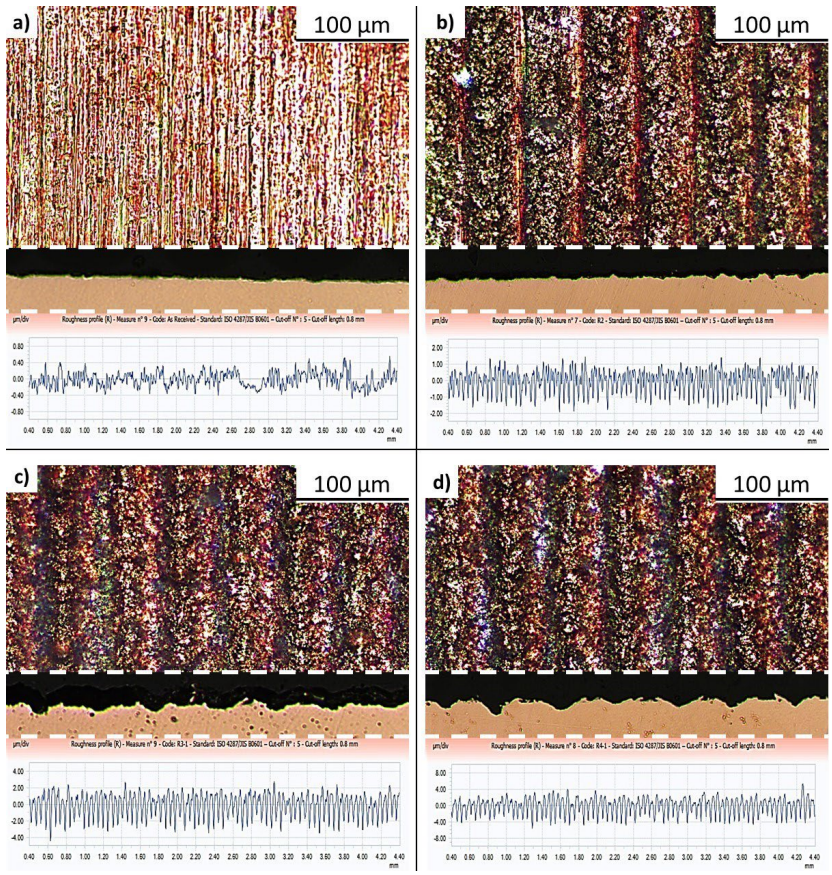


Fig. 2. Top view (top), cross-sectional view (middle), and roughness profiles (bottom) of (a) AR; (b) R1; (c) R2; (d) R3 surfaces.

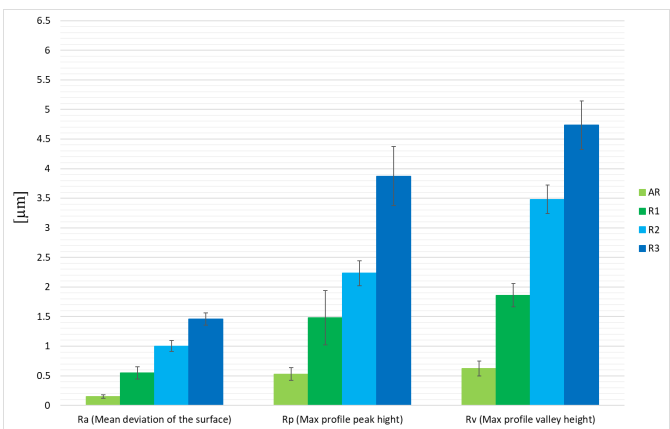


Fig. 3. Ra, Rp, and Rv measurement results for different surfaces.

This measurement substantiates the impact of laser-based texturing with low velocity and high-energy input to achieve a rough surface. It is evident that by reducing the velocity of the laser beam (see Table 1), a greater amount of energy is applied to the Cu surface, resulting in the ablation of more Cu material. The average surface roughness deviation (Ra) exhibits an increase from 0.5 µm (R1) to 1 µm (R2) and approximately 1.4 µm (R3). As anticipated, the as-received sample displays the smoothest surface. The measurement of the as-received surface (AR) reveals minimal values of 0.2 µm, 0.5 µm, and 0.6 µm for Ra, Rp, and Rv, respectively.

### *2.2. Temperature measurement*

Due to the physical limitation of the thermocouple attachment to the Cu surfaces for the temperature measurement, the configuration (as shown in Fig. 1) is selected. Consequently, the measured temperatures are proper indications of laser beam absorption by the Cu considering all the parameters except for surface condition are identical. However, the measured values are not usable to characterize the weld zone and the mechanical performance of the samples directly.

From the temperature measurement graphs (see Fig. 4), it can be observed that applying any surface structuring of R1, R2, or R3 results in a significant increase in the measured temperature. Considering all the parameters identical except for surface condition, the increase in temperature can be attributed to the improvement of the laser beam absorption by the Cu surface. Nevertheless, increasing the roughness values from R1 to R3 demonstrates a minor effect in comparison with the previously mentioned trend.

### *2.3. Laser welding*

Fig. 5 depicts the top view of the weld bead for different samples. They can be evaluated together with the shear load of the samples (see Fig. 6) as a complementary analysis to evaluate the beam absorption by the Cu surface and the stability of the keyhole. For laser-welded samples with as-received Cu surface, the welding is achievable only at 240 W of laser power. For lower powers in the as-received condition, no joint happens between Al and Cu due to the low absorption of the laser beam by the Cu surface. It is also in accordance with the temperature measurement as already described in Fig. 4.

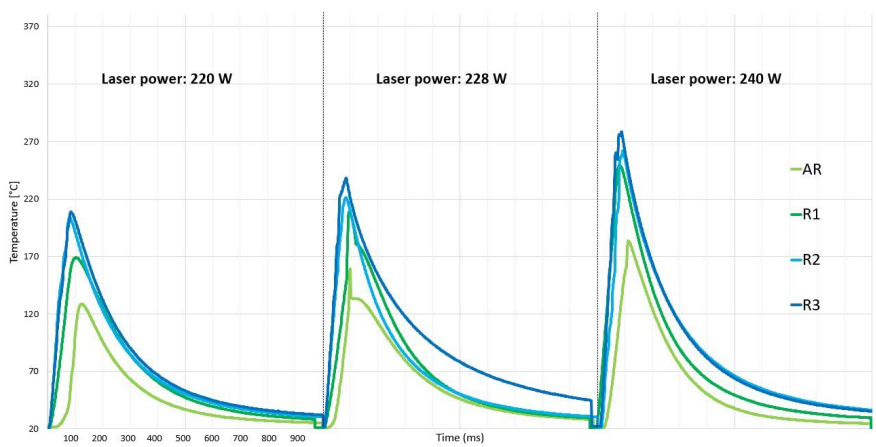


Fig. 4. Temperature measurement for different samples regarding power and surface condition.

Although the sufficient absorption of the laser beam for welding happens on the as-received samples at 240 W of power, it is merely at the end of the beam trajectory which is an indication of keyhole instability. It

is due to the increase of the temperature during the laser welding process, which facilitates the absorption process at the end of the beam path. Similar to the as-received category, for R1, R2, and R3 samples, by increasing the power, the appearance of the weld bead seems more uniform with less keyhole instability or lack of proper absorption, hence improving the beam absorption. Therefore, in addition to the AR-240 W sample, for R1-220 W, R2-220 W, and R3-220 W the keyhole instability is still problematic. R1-228 W sample shows an improvement of the keyhole stability compared to the corresponding welded sample with lower laser power and for R1-240 W, R2-228 W, R2-240 W, R3-228 W, and R3-240 W the weld bead presents sufficient absorption of the laser beam followed by the keyhole stability.

However, by evaluating Fig. 6, two different trends are observed for a fixed power with different surface conditions. At 220 and 228 W powers (which are not enough for welding the as-received samples), an increasing trend of the shear load from R1 to R2 samples followed by a decrease in the R3 is observed. Nevertheless, for 240 W, applying surface roughness deteriorates the shear load compared to the as-received surface regardless of the surface roughness values.

For the former trend, improvement of the beam absorption and keyhole stability has a positive effect on the shear load in the beginning which loses its effectiveness for high surface roughness values of R3 samples. For the latter trend at 240 W samples, except for the as-received one the others present very uniform weld bead and keyhole stability however, the mechanical performance of the corresponding welded samples is inferior.

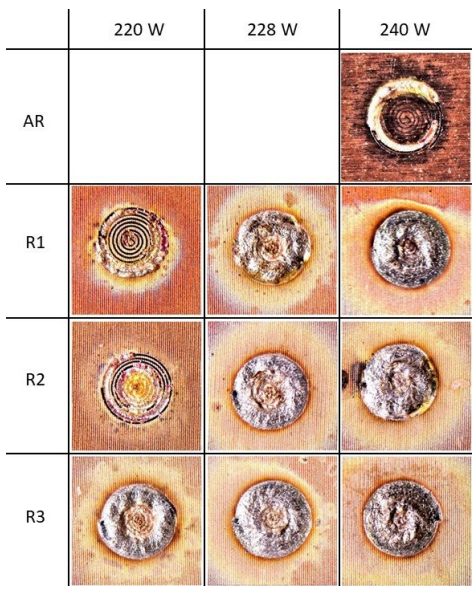


Fig. 5. Top view of the welding beads of different samples regarding power and surface condition.

The low value of the shear loads when the weld bead is inconsistent (keyhole instability), for instance, in the R1-220 W sample, is clearly due to the limited joining area between Al and Cu. However, for the samples with a uniform weld bead on Cu, i.e., the R2-240 W sample, the excessive amount of heat generated during the welding process provides a high melting volume of Cu and Al and intermixture of them. Consequently, by the formation of brittle intermetallic compounds (IMCs), the mechanical performance of the welds drops. In conclusion, there is an optimum range mitigating between keyhole stability (uniform bonding area between the materials) and the formation of IMCs, which presents the highest shear load.

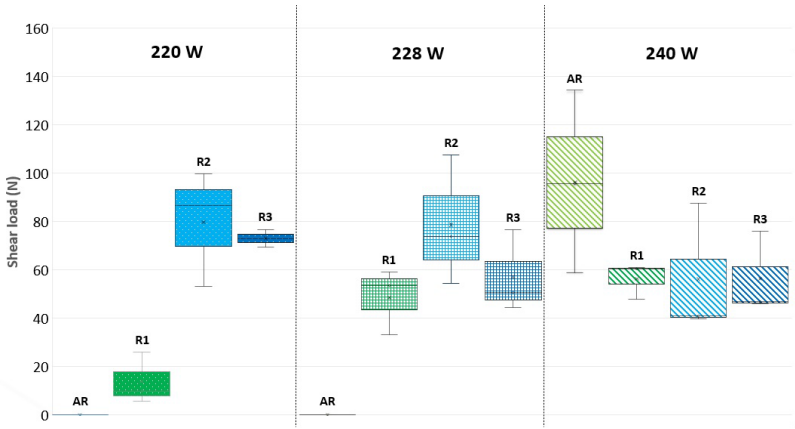


Fig. 6. The result of tensile-shear tests.

It is worth mentioning that some other experiments were implemented on samples with a higher range of surface roughness values (Ra ≈ 2 µm, Rp ≈ 4.6 µm, and Rv ≈ 5.7 µm). As the surface structuring for these samples is much more chaotic than the others, the absorption of the laser beam is suppressed. The weld bead appearance and the mechanical tests are not following the described trend and present a random behavior due to improper absorption of the laser beam by the Cu surface.

Fig. 7 represents the three types of failure happening during the tensile shear test. The first category is the mixture of no welded area and the failure in the Al near the weld. This typically happens in as-received condition welded with 240 W of laser power, R1, R2, and R3 samples welded with 220 W, and the value of the shear load is defined by the welding area at the interface of Cu/Al (under-weld samples). The second category of failure is for the samples that experience failure in the Al without observation of lack of welding i.e., R2-228 W (optimum weld). Finally, the last category addresses the samples with uniform, complete welding area between Cu and Al however, with reduced mechanical performance due to the formation of IMCs and the presence of cracks in the welding zone which results in the failure of both Cu and Al. For example, sample R2-240 W presents this type of failure (over-welded samples).

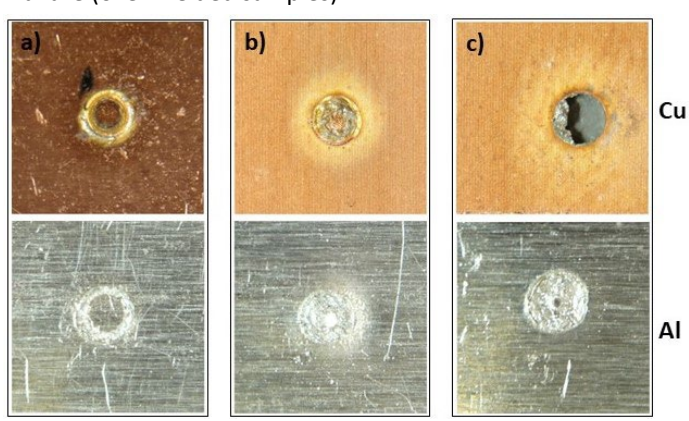


Fig. 7. Top view of the fractured samples after the tensile-shear tests, on top Cu, on the bottom, Al, a) mixed of Al failure and lack of weld, b) Al failure, c) mixed of Cu and Al failure.

### *2.4. Metallography*

Fig. 8 depicts some microscopic images of the cross sections for Cu-Al welded samples. Fig. 8-a and b show the cross sections of the as-received Cu sample welded to Al with 240 W of laser power before and after etching, respectively. These figures address the under-welding condition. No cracks are detected close to the weld, although a few voids are formed. In the vicinity of the Al boundary and weld zone, a transitional region exists where Al undergoes dissolution within the weld seam. This region is followed by a columnar dendritic structure, which is likely to be identified as the Θ phase $Al_2Cu$. Above this structure, there is a Cu-rich zone exhibiting a needle-like microstructure. The presence of a martensitic structure can be interpreted from the metastable transformation of the β-phase (Fig. 8-b), according to (Schmalen et al., 2019).

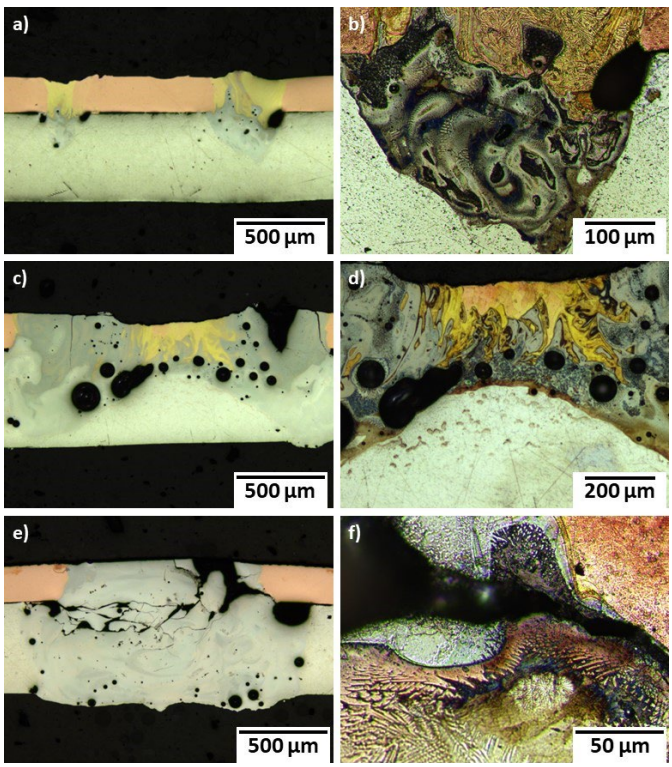


Fig. 8. Optical microscopic images of a) under-welded sample before chemical etching, b) the same sample after chemical etching, c) optimum-welded sample before etching, d) the same sample after etching, e) over-welded sample before etching, and f) the same sample after etching.

Fig. 8-c and d depict the R2-228 W sample before and after etching as representative of optimum-welded samples. There are some voids due to the evaporation of material with laser high-energy input in the weld zone. The middle of the weld displays an Al-bronze structure, easily discernible by its different color, transitioning gradually towards an orange color. Referring to (Schmalen et al., 2019), a uniform yellow area is observed at the center in the non-etched cross sections. However, a new metallurgical structure is revealed upon etching, taking on a needle-like shape between the Cu bronze and transition zone. This structure belongs to the γ-$Al_4Cu_9$ phase. As one moves away from the center of the weld in both left and right directions, the

depth of the weld increases. Small dark dendritic phases become visible in these regions, with a grain size of only a few microns. Adjacent to the Al on the lower side, a transition area of the eutectic point of (Al) + θ exists.

Fig. 8-e and f depict the cross section for the R3-240 W samples before and after etching as an example of the over-welded category. The unetched specimen depicted in Fig. 8-e exhibits a weld zone that has experienced a collapse, presenting numerous cracks and voids within it. Etching the polished metallography specimen for 1 minute reveals the presence of a dendritic structure known as the Θ phase $Al_2Cu$, previously investigated by (Zuo et al., 2014). This structure corresponds to a columnar dendritic pattern observed consistently across all weld seams. The dendrites exhibit peak-like formations with lengths between 3 and 70 µm (see Fig. 8-f). In addition, another structure similar to dendrites exists, but with a much shorter length, characterized by rounded morphology and a fine grain distribution with a few microns. This phase corresponds to the η phase, AlCu. Cracks are observed within and around this region.

## 3. Conclusions

In manufacturing automotive batteries, there is a requirement for dissimilar welding of materials, such as Cu-Al, with low thickness. However, various challenges arise during this process, including cracks, voids, inadequate bonding, and the formation of IMCs, which can result in low-quality welds. The findings presented in this paper demonstrate that infrared laser spot welding can serve as a valuable technology for achieving high-quality joints in materials with high reflectivity, such as copper. This is achieved through the implementation of laser-based structuring techniques prior to laser spot welding. The main conclusions drawn from this study are as follows:

- The technique of laser-based structuring was utilized to modify the surface roughness of thin copper sheets. As a result, a regular structure with average roughness values of approximately 0.5 mm, 1 mm, and 1.45 mm was achieved for surface conditions named R1, R2, and R3, respectively. Implementing laser-based structuring increased the absorption rate and molten volume under the spiral-shaped spot generated by a fiber laser operating at a wavelength of 1070 nm.

- The laser welding process of copper sheets with low thickness, 0.2 mm, presented certain challenges. Experimental findings indicate a narrow process window concerning the surface roughness (0.15-1.4 µm) and the laser power (220-240 W) for the spot laser welding process. Deviating beyond these specified ranges leads to the failure of the spot weld, resulting in undesirable defects such as cracks and voids within the welded zone. Results demonstrate that within the power range of 220-228 W, R2 exhibits the maximum mechanical strength owing to an increment in absorption. However, at the high laser power of 240 W, an increase in the surface roughness leads to elevated absorption and subsequent over-welding, resulting in reduced mechanical strength.

- Metallographic analysis of the specimens reveals the presence of intermetallic compounds. Upon etching, the over-welded samples exhibit a dendritic structure consisting of the Θ phase, $Al_2Cu$, and another phase interpreted as η phase, AlCu, which displays susceptibility to cracking in this region. Furthermore, in the case of the optimally welded samples, IMCs are minimized, however, a needle-like structure comprising the γ-$Al_4Cu_9$ phase is observed.

## References

Amne Elahi, M. and Plapper, P. (2019) “Dissimilar Laser Micro-Welding of Nickel Wire to CuSn6 Bronze Terminal”, Transactions of the Indian Institute of Metals, 72(1), pp. 27–34. Available at: https://doi.org/10.1007/s12666-018-1457-y.

Biro, E., Weckman, D.C. and Zhou, Y. (2002) “Pulsed Nd:YAG laser welding of copper using oxygenated assist gases”, Metallurgical and Materials Transactions A, 33(7), pp. 2019–2030. Available at: https://doi.org/10.1007/s11661-002-0034-4.

Brand, M.J., Schmidt, P.A., Zaeh, M.F. and Jossen, A. (2015) “Welding techniques for battery cells and resulting electrical contact resistances”, Journal of Energy Storage, 1(1), pp. 7–14. Available at: https://doi.org/10.1016/j.est.2015.04.001.

Chen, H.C., Bi, G., Nai, M.L.S., and Wei, J. (2015) “Enhanced welding efficiency in laser welding of highly reflective pure copper”, Journal of Materials Processing Technology, 216, pp. 287–293. Available at: https://doi.org/10.1016/j.jmatprotec.2014.09.020.

Dong, P. and Xiao, R. (2009) “Laser welding of lap joint between copper and brass”, in International Congress on Applications of Lasers & Electro-Optics. Laser Institute of America, pp. 203–207. Available at: https://doi.org/10.2351/1.5061553.

Engler, S., Ramsayer, R. and Poprawe, R. (2011) “Process Studies on Laser Welding of Copper with Brilliant Green and Infrared Lasers”, Physics Procedia, 12, pp. 339–346. Available at: https://doi.org/10.1016/j.phpro.2011.03.142.

Heider, A., Weber, R., Herrmann, D., Herzog, P. and Graf, T. (2015) “Power modulation to stabilize laser welding of copper”, Journal of Laser Applications, 27(2), p. 022003. Available at: https://doi.org/10.2351/1.4906127.

Helm, J., Schulz, A., Olowinsky, A., Dohrn, A. and Poprawe, R. (2020) “Laser welding of laser-structured copper connectors for battery applications and power electronics”, Welding in the World, 64(4), pp. 611–622. Available at: https://doi.org/10.1007/s40194-020-00849-8.

Hess, A., Schuster, R., Heider, A., Weber, R. and Graf, T. (2011) “Continuous wave laser welding of copper with combined beams at wavelengths of 1030 nm and of 515 nm”, in Physics Procedia. Elsevier B.V., pp. 88–94. Available at: https://doi.org/10.1016/j.phpro.2011.03.012.

Kaierle, S., Overmeyer, L., Hoff, C., Herzorg, P. and Hermsdorf, J. (2016) “Conditioning of copper material surfaces increasing the efficiency of continuous wave laser microwelding”, CIRP Journal of Manufacturing Science and Technology, 14, pp. 66–70. Available at: https://doi.org/10.1016/j.cirpj.2016.05.006.

Lee, K. and Ki, H. (2021) “Enhancing coupling efficiency in laser keyhole welding of copper using femtosecond laser surface modification”, Optics and Laser Technology, 139. Available at: https://doi.org/10.1016/j.optlastec.2021.106943.

Maina, M., Okamoto, Y., Inoue, R., Nakashibe, S., Okada, A. and Salagawa, T. (2018) “Influence of Surface State in Micro-Welding of Copper by Nd:YAG Laser”, Applied Sciences, 8(12), p. 2364. Available at: https://doi.org/10.3390/app8122364.

Norouzian, M., Amne Elahi, M. and Plapper, P. (2023) “A review: Suppression of the solidification cracks in the laser welding process by controlling the grain structure and chemical compositions”, Journal of Advanced Joining Processes. Elsevier B.V. Available at: https://doi.org/10.1016/j.jajp.2023.100139.

Schmalen, P., Mathivanan, K. and Plapper, P. (2019) “Metallographic Studies of Dissimilar Al-Cu Laser-Welded Joints Using Various Etchants”, Metallography, Microstructure, and Analysis, 8(1), pp. 3–11. Available at: https://doi.org/10.1007/s13632-018-0501-y.

Steen, W.M. and Mazumder, J. (2010) Laser Material Processing. London: Springer London. Available at: https://doi.org/10.1007/978-1-84996-062-5.

Zuo, D., Hu, S. and Shen, J. (2014) “Intermediate layer characterization and fracture behavior of laser-welded copper/aluminum metal joints”, Materials & Design, 58, pp. 357–362. Available at: https://doi.org/10.1016/j.matdes.2014.02.004.